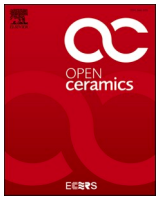
Open Ceramics 18 (2024) 100579



Contents lists available at ScienceDirect

Open Ceramics

journal homepage: www.sciencedirect.com/journal/open-ceramics





Electronic and thermal properties of Nb_2CCl_2 MXenes

H. Pazniak [a,*], T. Ouisse [a], U. Wiedwald [b], J. Gonzalez-Julian [c], T. Ito [d], F. Wilhelm [e], A. Rogalev [e], S. Quessada [a]

[a] Université Grenoble Alpes, CNRS, Grenoble INP, LMGP, Grenoble, France
[b] Faculty of Physics and Center for Nanointegration (CENIDE), University of Duisburg-Essen, Duisburg, Germany
[c] Chair of Ceramics, Institute of Mineral Engineering, RWTH Aachen University, Germany
[d] Nagoya University Synchrotron Radiation Research Center (NUSR), Nagoya University, Nagoya, Japan
[e] European Synchrotron Radiation Facility (ESRF), Grenoble, France

ARTICLE INFO

Handling Editor: Dr P Colombo

ABSTRACT

The molten salt synthesis has recently opened up new opportunities to functionalize two-dimensional MXenes with uniform halogen terminations. In this work, we synthesize Nb_2CCl_2 MXenes by etching the Al layer from the Nb_2AlC precursor in the melt of $CuCl_2$ Lewis acid. In Cl-terminated MXenes, intercalation of water is negligible, so that MXenes get closer to ideal, ordered van der Waals solids. We identify the preferential atomic stacking arrangement, which is of the AB type, as opposed to the AA stack assumed in previous works. We combine X-ray absorption near edge spectroscopy with density functional theory to clarify the local chemical environment of Cl atoms. Using vibrating sample magnetometry and specific heat measurements, we confirm that Nb_2CCl_2 MXenes are superconducting with a transition temperature of 6.0 K and find a Debye temperature of 320 K. We further show that the transition temperature slightly decreases with applied isostatic pressure.

1. Introduction

MXenes are a chemically diverse class of two-dimensional (2D) materials that has been discovered in 2011. These phases show promising application in many fields including supercapacitors, energy storage, catalysts, gas detectors and biosensors [1]. MXenes are hexagonal, a few atomic layers thick and composed of early transition metals (M) and carbon or nitrogen atoms (X). The symmetry of MXenes is inherited from the bulk 3D precursor, the MAX phase, which in addition contains an A layer (usually Al, Si, or Ga) that alternates between the MX slabs [2]. Due to the different nature of chemical bonds in the crystal structure of the MAX phase precursor, the A layer can be selectively etched by different methods. Initially, the synthesis of MXenes was carried out by selective chemical etching in a HF solution [3]. Further extensive research has led to the development of alternative "safe" etchants and etching routes for the synthesis of MXenes [4–7]. While most synthesis methods take place in an aqueous environment and results in mixed surface terminations that are typically = O, –OH, and –F, etching in molten salts is conducted in the melt of inorganic compounds at elevated temperatures and results in uniform halogen terminations. Compared to mixed-terminated, molten salt etched MXenes are more resistive to oxidation [8], however, the most intriguing is that the surface termination T_x (halogen and chalcogenide) lead to the superconductivity of the Nb_2CT_x phase [6,9]. The transition temperature (T_c) of Nb_2C MXenes shows a strong dependence on the nature of surface groups and varies from 7.1 K for bare Nb_2C(NH)-terminations to 4.5 K for Se-terminations [6]. It has recently been shown that replacement of surface functional groups with nitrogen atoms can alternatively induce superconductivity in mixed-terminated Nb_2CT_x MXenes with an increase in T_c as the flake or film thickness increases [10]. Superconductivity of bulk materials is generally established by the interplay of the electronic density of states at the Fermi level, the characteristic phonon frequency, and the electron-phonon coupling. In case of intermetallic superconductors with a lattice instability, the superconducting properties including T_c can be altered by applying isostatic pressure, which drives materials towards or away from the lattice instability [11].

In case of 2D materials, pressure is also an effective parameter that allows to change the interlayer distance, the van der Waals interaction and the electronic states, which define their physical properties. It has been experimentally confirmed that high pressure induces superconductivity in other 2D systems such as WTe_2 and ZrS_2 [12] and excitonic transition in bilayer MoS_2 [13]. In case of MXenes, it has been

* Corresponding author.
E-mail address: hanna.pazniak@grenoble-inp.fr (H. Pazniak).

https://doi.org/10.1016/j.oceram.2024.100579
Received 9 February 2024; Received in revised form 16 March 2024; Accepted 18 March 2024
Available online 19 March 2024
2666-5395/© 2024 The Authors. Published by Elsevier Ltd on behalf of European Ceramic Society. This is an open access article under the CC BY-NC-ND license (http://creativecommons.org/licenses/by-nc-nd/4.0/).

theoretically predicted that the electronic structure of Ti_2C MXenes functionalized with = O surface groups changes under pressure. At zero pressure, they show a band gap of 0.9 eV which gradually decreases with increasing pressure and vanishes at about 7 GPa [14]. In this case the metallic character of Ti_2CO_2 mainly results from a strong interaction between Ti-*d* and C-*p*, and Ti-*d* and O-*p* states [14]. Pressure-dependent electronic transport properties have also been measured for superconducting Nb_2CCl_2 MXenes [15]. Surprisingly, the study showed no change of T_c under pressure, only an overall decreasing resistance has been observed. Note that Nb_2CT_x MXenes with mixed terminations (T_x = –OH; –F; =O) are not superconducting at pressures of up to 40 GPa. Nb_2CT_x MXenes have been shown to be very promising for biomedical application, particularly for cancer phototherapeutic applications in first and second near infrared light bio-windows [16]. Given the higher stability of Nb_2CCl_2 MXenes compared to Nb_2CT_x, they are of great interest for testing in such applications.

In this study, we present the synthesis of superconducting Nb_2CCl_2 MXenes and study their structural, electronic and thermal properties. The transition temperature of Nb_2CCl_2 was determined by vibrating sample magnetometry (VSM) and specific heat capacity measurements. We studied the local chemical environment of Cl atoms by X-ray absorption near edge spectroscopy at the K-edge of Cl complemented by density functional theory and find a strong hybridization of Cl and Nb electronic states. In addition, we studied the pressure dependence of superconductivity in Nb_2CCl_2 MXenes. In contrast to previously published data [15], we observed a continuous decrease of T_c as function of pressure up to 1.3 GPa. Besides, we report for the first time the thermal properties of Nb_2CCl_2 MXenes, including heat capacity and Debye temperature, the experimental value of which is determined to be 320 K and is within the range of theoretically predicted values.

2. Materials and methods

2.1. Material synthesis

Nb_2CCl_2 MXenes were produced by selective chemical etching of Al layer from Nb_2AlC MAX phase in a melt of inorganic salts composed of copper (II) chloride ($CuCl_2$, anhydrous, 99.995%) as an etching agent and a mixture of sodium chloride (NaCl, anhydrous, 99.995%) and potassium chloride (KCl, anhydrous, 99.995%) as a supporting salt bed [17]. The components were mixed in a ratio of 1 : 5: 2 : 2 in a mortar and pestle in inert atmosphere. The mixture was then placed in an alumina crucible, covered with a lid, and transferred to a quartz tube of a tubular furnace (Eraly&Associes, France). The synthesis was carried out at 700 °C for 6 h and a heating rate of 5 °C/min in argon atmosphere followed by free cooling to room temperature. The sintered material was removed from the crucible and mixed with deionized (DI) water to dissolve residual salts, and then washed with DI water followed by centrifugation. The collected sediment composed of black powder and reddish particles of elemental Cu. The latter has been removed by washing in a diluted ammonium persulfate (APS) ($(NH_4)_2S_2O_8$, 99.995%) solution (0.1 M) for 30 min. The resulting suspension was centrifuged several times, and the sediment was collected and left for drying.

2.2. Structural characterization

The Nb_2AlC MAX phase precursor and Nb_2CCl_2 powder were studied by X-ray diffraction (XRD) using a D8 Bruker diffractometer (Bruker, Massachusetts, USA) operating under the Bragg-Brentano geometry and equipped with Cu anode providing X-rays with a wavelength of 1.5406 Å. The morphology and chemical composition of the synthesized powder was investigated using a field-emission scanning electron microscopy (SEM) (ZEISS Gemini 300, Carl Zeiss AG, Oberkochen, Germany) equipped with a Si(Li) detector (Oxford Instruments) for energy dispersive X-ray spectroscopy (EDS). The multilayer MXene powder was sonicated in isopropyl alcohol for 10 min and drop-casted onto a Cu grid for transmission electron microscopy (TEM) using a JEOL 2200FS microscope at an acceleration voltage of 200 kV using a 2k × 2k GATAN UltraScan1000XP CCD camera. The local chemical composition was determined using EDS in STEM mode with an Oxford windowless 80 mm^2 SDD X-MaxN 80 TLE detector with 0.21 sr solid angle. X-ray Absorption Near Edge Spectroscopy (XANES) at the Cl K-edge was measured at room temperature at the European Synchrotron Radiation Facility (ESRF) ID12 beamline [18] using the partial fluorescence yield (PFY) detection mode with a silicon drift detector mounted in backscattering geometry.

2.3. Computational details

Computations were based on Density Functional Theory (DFT) as implemented in the Wien2k package, using the linearized augmented plane wave + local orbitals (LAPW + lo) method. Non-local van der Waals forces between two adjacent Cl atomic planes were taken into account through the use of the GGA Perdew, Burke and Ernzerhof (PBE) + rVV10L functional, previously reported to be appropriate for modelling layered, van der Waals solids [19]. A 58 × 58 × 9 Monkhorst Pack grid was used. XRD data provided the input lattice parameter values, and all relative atomic positions were optimized (muffin tin radii were initially reduced by 5% with respect to the maximum possible values allowed by the crystal structure). XANES were computed in the dipole approximation, using the XSPEC module implemented in the Wien2k package. For this, a 2 × 2 × 1 supercell was built and a core hole was introduced on just one Cl atom site, compensated by a uniform negative charge background, for carrying out the self-consistent calculation required before computing the XANES spectra. Xcrysden was used for computing the Fermi Surface [20].

2.4. Physical properties measurements

Pressure-dependent magnetometry was performed using a PPMS DynaCool system (Quantum Design) using a Beryllium Copper cylindrical cell (Quantum Design). Nb_2CCl_2 powder was placed in a Teflon tube along with transmitting media oil and manometer. The pressure calibration has been done via a piece of Sn with known $T_c(P)$ as function of pressure. The experimentally determined relation for Sn, $T_c(P) = 3.73$ K - 0.4823 P - 0.0207•P^2 has been used as suggested by Eiling and Schilling [21]. Two runs with two different fields and temperature sweep rates have been measured. Specific heat was measured using a PPMS DynaCool system using the heat capacity option. The Nb_2CCl_2 sample was pressed into a cylindrical shape with a diameter of 3 mm by a hydraulic press and then mounted to a calorimeter puck using a small amount of vacuum grease.

3. Results and discussion

3.1. Nb_2CCl_2 synthesis and characterization

Nb_2CCl_2 was produced via molten salt etching as detailed in the Materials and Methods Section. In short, Nb_2AlC fine powder was mixed with inorganic salts of $CuCl_2$, NaCl and KCl, then the mixture was heated up to 700 °C. During synthesis, Cu^{2+} oxidizes Al from Nb_2AlC, causing further interaction with Cl^- and gaseous $AlCl_3$ is released as a product. The oxidation of aluminum is balanced by subsequent reduction of Cu^{2+} to elemental copper. After synthesis, the material in the crucible appears as a solidified melt with a characteristic reddish-brown color, indicating the presence of elemental copper. The latter is then removed from the material, leaving only black powder of multilayered Nb_2CCl_2.

First, the multilayered Nb_2CCl_2 powder was characterized by XRD. The data shows that after synthesis, the (002) peak of Nb_2AlC shifts towards lower 2θ angles, indicating a change in the c-lattice parameter from 13.88 Å to 17.42 Å (Fig. 1a). This is due to the removal of the

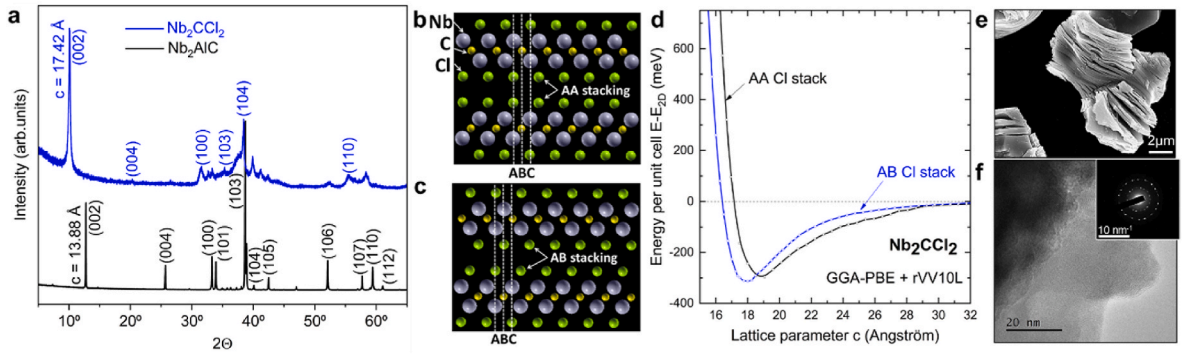


Fig. 1. Characterization of Nb_2CCl_2 MXenes. **a)** XRD patterns of Nb_2AlC MAX phase precursor and Nb_2CCl_2 MXenes; **b), c)** van der Waals AA and AB atomic stacking arrangement, respectively; **d)** Energy as a function of c lattice parameter; **e)** SEM image of Nb_2CCl_2 multilayers; **f)** TEM image of Nb_2CCl_2 multilayer with the corresponding SAED pattern (inset).

aluminum layer and the surface functionalization with Cl terminations in the multilayer MXenes. We compared this experimental value with the DFT values predicted for two different configurations of two adjacent Cl planes. The first one, which we name *AA* stack, corresponds to the Cl atoms occupying the same hcp sites in both planes (Fig. 1b). This configuration is the one considered in Ref. [6] and some subsequent articles [9]. In the second configuration, which we name *AB* stack, the Cl atoms of the upper planes are shifted to B site, so that each Cl atom of the upper (lower) plane interacts with 3 Cl atoms in the lower (upper) plane (Fig. 1c). We took into account van der Waals interactions by using the GGA-PBE + rVV10L functional, shown to be well suited to the study of van der Waals solids [19]. Plotting the overall energy per unit cell as a function of the lattice parameter **c**, while relaxing all relative atomic positions for each **c** value, show that the AB configuration displays a lower energy minimum, and a smaller lattice parameter (17.9 Å versus 18.9 Å, respectively, see Fig. 1d), much closer to the experimental value found by XRD.

Such a residual discrepancy (a slightly larger theoretical lattice parameter) was already noticed by investigating many van der Waals solids with the same functional [19]. This result suggests that (i) the most stable configuration is of the *AB* type and (ii) there is (almost) no intercalated water or other intercalants between MXene sheets, which may affect the physical properties [22]. It is worth noticing that the *AA* and *AB* configurations display very similar band structure and Fermi Surface (FS), so that, most probably, the way how the MXenes are stacked should not have a major impact on the superconducting properties. In comparison, the c-lattice parameter of Nb_2CT_x MXenes with mixed –OH, –F, and = O termination produced by wet chemistry in a mixture of LiF and HCl is about 24.05 Å [23], which is considerably larger than what is observed with Cl termination despite the ionic radii of O and F is smaller the one of Cl. Another interesting point is that the (002) peak is very narrow as compared with mixed-terminated Nb_2CT_x MXenes [23], indicating more regular interlayer spacing throughout the sample in case of surface functionalization with Cl surface groups. At the same time, we also observed an increased a-lattice parameter from 3.05 Å to 3.29 Å as revealed by the selected area electron diffraction (SAED) patterns (Fig. 1f, inset), which is consistent with other experimental reports on Cl-terminated MXenes [6]. The a-lattice parameter of Nb_2CCl_2 MXenes is much larger than that of mixed-terminated Nb_2CT_x (3.087 Å) [15]. It was found that after synthesis, Nb_2CCl_2 has an expanded multilayered structure, typical to other MXenes produced via molten salt etching as a result of the release of gaseous $AlCl_3$ (Fig. 1e). The chemical composition of the Nb_2CCl_2 powder, measured by EDS, contains tiny amounts of Al (0.57 at.%) and Cu (0.89 at.%), which confirms successful removal of aluminum during synthesis and copper particles during washing in APS, respectively. The average ratio of Nb/Cl was found to be 2/1.55, which is lower than the nominal value of 2/2, which is assumed to occur when the MXene surface is saturated with Cl terminations [24]. Deviations from the expected ratio may be due to the presence of oxygen groups that partially replace Cl when washing the powder with APS, or due to the surface defects [6]. However, by using a low-concentration APS solution (0.1 M) for a relatively short time, the amount of oxygen, detected by EDS, does not exceed 5 at. % (despite the transfer in air), which is significantly lower compared to the same washing procedure using a more concentrated APS solution [17]. The TEM image of Nb_2CCl_2 shows a stack of several translucent flakes arranged in the form of a multilayer with thin edges and more bulky regions in the middle of the multilayer (Fig. 1f). The SAED pattern, recorded in the thinnest region, reveals a hexagonal structure with high crystallinity, visible as well-defined and sharp spots.

To study the chemical environment of Cl atoms, we have performed XANES at the Cl K-edge. Due to the element specificity of XANES determining the density of unoccupied states, we can directly probe the Cl K-edge, which corresponds to electron excitation from the Cl 1s orbital to molecular orbitals of hybridized Cl 3p and d orbitals of transition metals. This allows us to accurately monitor the changes in chemical bonding induced by functionalization. The normalized XANES spectrum of Nb_2CCl_2 MXenes is presented in Fig. 2a (black curve). To record this spectrum, we have pressed a thin pellet of Nb_2CCl_2 powder and placed it on a sample holder so that the surface normal is nearly perpendicular to the incoming X-ray beam. When performing XANES, we switched the linear polarization (from vertical to horizontal using a 5 μm Si quarter wave plate) to access in-plane and out-of-plane orientation of Cl atoms. However, due to the fact that multilayered MXene powder was used, the experimental XANES spectra are found to be independent of the linear polarization. The experimental XANES spectrum shows a well-defined pre-edge peak at 2822.7 eV. This feature indicates a direct bonding of Cl ions with Nb and reveals a high covalency of the bond [25]. The spectrum shows additionally three peaks at 2825.0 eV, 2828.6 eV, and 2830.7 eV.

For the detailed interpretation of XANES spectra we have performed DFT calculations considering different orientations of the MXene stack with respect to the X-ray polarization vector. As expected from the crystal structure anisotropy, the calculated spectra substantially differ, depending on whether the incident light beam linear polarization lies in- or out-of-plane (along the c-axis or (a,b)-plane) (see Fig. 2a). The first absorption peak, around 2822.7eV, is present in both cases but, for instance, a second peak around 2825.0 eV is predicted to appear only in the case of the out-of-plane, p_Z-contributed spectrum (Fig. 2a). And other peaks prevalently appear just for one of the two configurations. However, the experimental spectrum, measured with in-plane polarization, noticeably differs from the calculated ones. This is ascribed to the substantial orientation disorder induced by random MXene grain orientations probed by X-ray absorption experiment (the probing depth is less than 1 μm at the Cl K-edge), even if horizontal stacking is somewhat favored as can be seen from the XRD pattern (Fig. 1a), where the peak

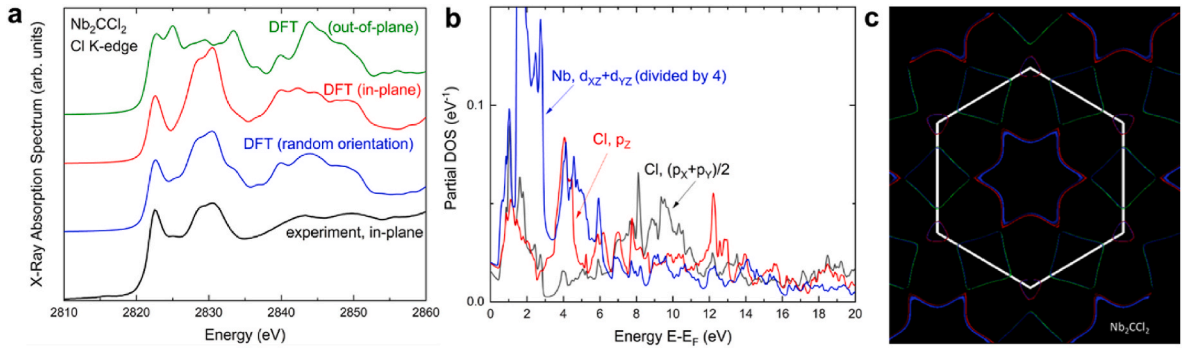


Fig. 2. a) DFT-based and experimental XANES, computed or measured for different orientations of MXenes with respect to linearly polarized X-rays. DFT was computed using a 2 × 2 × 1 supercell including a core hole; **b)** Partial density of states (DOS) of selected Cl and Nb orbital contributions as a function of energy; **c)** Fermi surface viewed from « top » (c-axis is orthogonal to the figure plane); the appearance of the Fermi Surface in the form of simple lines shows that the compound, even stacked in a van der Waals crystal, remains very close to a 2D electronic system.

originated from (00*l*) planes have highly increased intensities as compared to the peaks originated from in-plane (100) and (110) orientations. Additionally, the (002) peak broadening is reminiscent of this degree of disorder. Remarkably enough, assuming a random crystal orientation gives a very reasonable agreement between DFT-based and experimental X-ray absorption spectra (see Fig. 2a). This good agreement further indicates a rather random orientation of MXene multilayers in the pressed powder sample and gives confidence that DFT provides reasonable results for further interpreting the data. A plot of some partial densities of states (p-DOS) is given in Fig. 2b. It is striking that the XANES peaks are directly correlated to the peaks in the p-DOS plots of either the $3p_X+3p_Y$ orbitals, or $3p_Z$ orbitals. Besides, comparing the Cl and Nb-based DOS also shows that both are highly correlated, indicating that the measured Cl absorption spectrum allows us to probe the 4*d*-Nb-3*p*-Cl hybridization. Unfortunately, none of the Cl peaks appears to be fully uncorrelated with the DOS of Nb which would allow one to discriminate experimentally between the Nb–Cl bonds and the Nb–Nb interactions between two Nb adjacent planes.

3.2. *Electronic and thermal properties of Nb_2CCl_2 MXenes*

We further investigated the electronic and thermal properties of the synthesized Nb_2CCl_2 MXenes. First, we measured the field-dependent magnetization at different temperatures by vibrating sample magnetometry. Fig. 3a presents the data after removal of paramagnetic slopes. For all temperatures below T_c we observe the typical diamagnetic response of a superconductor from 0 T to 0.02 T. Above 0.02 T, the M(B) curve begins to deflect from the linear behavior and parabolically decreases and then asymmetrically increases with increasing field indicating the penetration of magnetic fields through vortices. The observed behavior is typical for a Type II superconducting material. With increasing temperature from 2.5 K to 7.0 K, the absolute values of magnetization decrease (in a field of 0.02 T) and at $T_c = 6$ K the negative magnetization indicating the superconducting state approaches zero

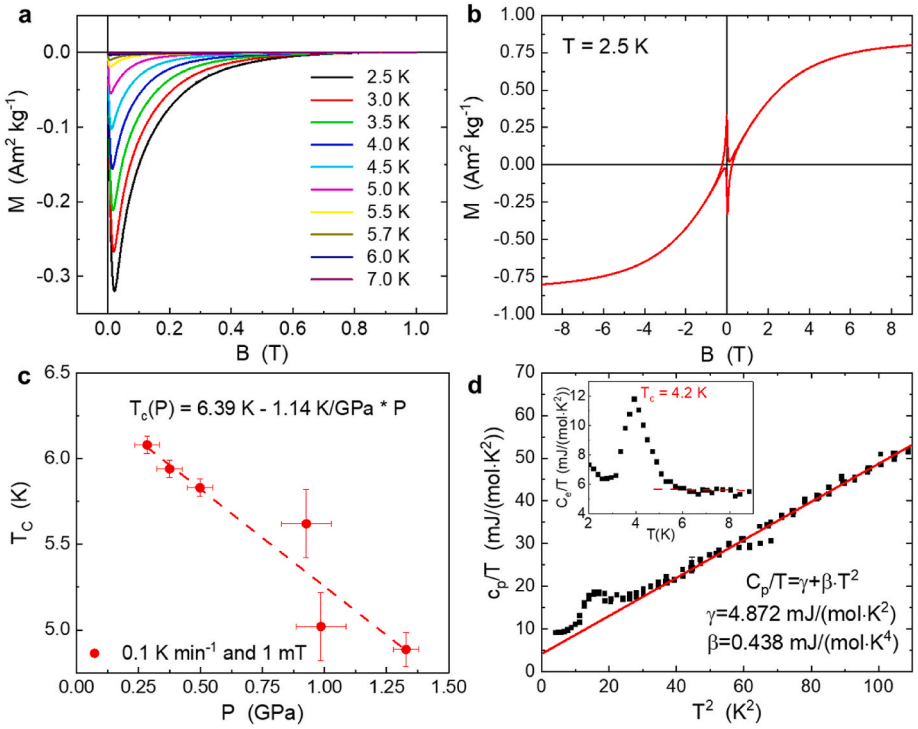


Fig. 3. Physical characterization of Nb_2CCl_2 MXenes. **a)** Magnetization (M) versus applied magnetic field at various temperatures after subtraction of paramagnetic slopes; **b)** Superconducting hysteresis loop at 2.5 K; **c)** T_c of Nb_2CCl_2 MXenes as a function of applied pressure; **d)** Heat capacity of Nb_2CCl_2 MXenes as function of temperature in C_p/T (T^2) scaling.

values. The determined T_c is in the same range as for Nb_2CCl_2 MXenes synthesized using $CdCl_2$ Lewis acid (5.2 K–6 K) [6,9]. To determine the upper critical field, we recorded hysteresis loops at various temperatures below T_c. The M(B) curve at 2.5 K and ±9 T is shown in Fig. 3b. The hysteresis has a typical shape for superconducting materials and the corresponding diamagnetic response disappear at fields larger than 0.7 T.

We further investigated the superconducting behavior of Nb_2CCl_2 MXenes as a function of isostatic pressure as shown in Fig. 3c. We considered the pressure range from 0 GPa to 1.3 GPa that can be achieved in a PPMS device using the pressure cell option for magnetometry. We observed an almost linear decrease of T_c with applied pressure, and at a maximum applied pressure of 1.3 GPa, T_c is about 4.8 K. We note here that many of the superconducting metallic elements, e.g. Pb, Sn, In show a decreasing T_c with pressure [21]. This negative pressure coefficient is often attributed to the volume dependence of the electronic density of states at the Fermi energy and of the effective interaction between the electrons mediated by the electron-phonon coupling [11]. Similar to conventional superconductors [26], we attribute the decrease in T_c in Nb_2CCl_2 MXenes with the phonon stiffening induced by pressure, the effect from which overcomes the effect related to the change in electronic properties. The same behavior has been observed for 2D hexagonal β-Mo_2C [26]. However, the pressure-dependent superconducting behavior of Nb_2CCl_2 MXenes observed in our study contradicts previously published results. H. Jin et al. [15] found that with increasing pressure to 41.5 GPa, only the width of the superconducting transition continues to expand, while maintaining the superconducting nature of the material. We attribute this difference to the different experimental techniques used to characterize the superconducting state. H. Jin et al. [15] studied pressure-dependent superconductivity using four-probe resistance measurements, which are known to be much more sensitive to the in-plane transport in 2D MXenes. In our study, we used magnetometry, which reflects the response of the entire sample.

Next, we measured the heat capacity in the temperature range 2.5–15 K. Fig. 3d shows a plot of C_p/T versus T^2, between 2.5 K and 10 K. Similar to the magnetic measurements (Fig. 3a), we observed a temperature-dependent anomaly in the form of a sharp jump of the heat capacity in the low temperature region confirming the superconducting nature of Nb_2CCl_2 MXenes. We then fit the linear region (above T_c) of C_p/T to $C_p = \gamma T + \beta T^3$, where the first term represents the electronic heat capacity (electronic contribution) and the second accounts for the lattice heat capacity (phonon contribution). The red solid line (Fig. 3d) is the resulting linear fit to the C_p/T versus T^2 data, giving the Sommerfeld coefficient $\gamma = 4.872$ mJ/(mol·K^2) and the phonon contribution $\beta = 0.438$ mJ/(mol·K^4). By subtracting the latter from the total heat capacity (C_p - $\beta \cdot T^3$), we obtain the electronic specific heat $C_e(T)$ as a constant and deviations indicate the onset of superconductivity. The inset in Fig. 3d shows C_e/T as a function of T. It reveals a rather broad distribution of T_c between the peak position at 4.2 K and 6 K above which the normal Sommerfeld heat capacity is obtained. Such distribution could be explained by a high sensitivity of the superconducting state (and thus T_c) to defects (missing Cl terminations) and a small amount of = O terminations from the sample preparation (as revealed by EDS).

Using the fitted values of Sommerfeld coefficient, γ, and phonon coefficient, β, we calculate an experimental density of states (DOS) at the Fermi energy $D(E_F)$ and the Debye temperature Θ_D using the following equations: $\gamma = \pi^2 N_A \kappa_B^2 / 3D(E_F)$ and $\beta = 12\pi^4 N \kappa_B / 5\Theta_D^3$ [27]. As a result, $D(E_F)$ of Nb_2CCl_2 is 4.05 states/eV per unit cell, quite comparable with the values assessed for many MAX phases [28] and Θ_D is 320 K. The experimental value of the Debye temperature of Nb_2CCl_2 found in our study is close to theoretical values predicted by R. Khaledialidusti et al. (296 K for Ti_2CO_2) [29] and P. Francisco-Santiago et al. (336–343 K for Ti_2CO_2, Ti_2CCl_2 and Ti_2NCl_2) [30]. Taking into account the theoretical value found from the DFT, $D_{DFT}(E_F) = 2.4845$ states/eV per unit cell, we can assess an electron-phonon coupling constant as $\lambda = D(E_F)/D_{DFT}(E_F) - 1 = 0.63$, similar to the values found for early transition metals and MAX phases. Remarkably enough, this is also the same value as estimated for Nb_2CCl_2 in Ref. [9] from McMillan formula, using a DFT estimation of the logarithmic averaged phonon frequency and an assumed value of the coulomb repulsion potential. With the hope of getting more insight into the reasons why Nb_2CCl_2 is superconducting, we also examined the Fermi surface (FS) shape (Fig. 2c). The FS is almost 2D, and some flat parts parallel to **c** inside the first Brillouin zone are almost parallel to each other, which, combined with the quasi 2D character and relatively high DOS at E_F, could be factors favoring superconductivity. However, these considerations are not sufficient, since the FS of Nb_2CF_2, which we computed in the same way, is very similar to that of Nb_2CCl_2, whereas the former phase is not superconducting. Therefore, the difference very probably lies in the different halide masses and the way they shape the phonon dispersions and the electron-phonon coupling.

4. Conclusions

In conclusion, we have synthesized Nb_2CCl_2 MXenes via molten salt etching from Nb_2AlC MAX phase precursors. By detailed structural and electronic characterization supplemented by theoretical calculations, we revealed a strong Nb–Cl hybridization in the MXenes. Moreover, we propose that XANES at the Cl K-edge can be used as an accurate tool to determine the anisotropy of Cl-based MXenes in combination with DFT. Both, magnetic and heat capacity measurements, confirmed a superconducting behavior of the synthesized Nb_2CCl_2 MXenes with transition temperature up to 6 K. Pressure-dependent magnetometry showed a slight decrease in the transition temperature with applied pressure.

CRediT authorship contribution statement

H. Pazniak: Investigation, Supervision, Writing – original draft, Writing – review & editing, Conceptualization. **T. Ouisse:** Investigation, Visualization, Writing – review & editing, Conceptualization. **U. Wiedwald:** Formal analysis, Investigation, Writing – review & editing, Conceptualization. **J. Gonzalez-Julian:** Resources, Writing – review & editing. **T. Ito:** Investigation, Writing – review & editing. **F. Wilhelm:** Formal analysis, Investigation, Writing – review & editing. **A. Rogalev:** Formal analysis, Investigation, Writing – review & editing. **S. Quessada:** Resources, Writing – review & editing.

Declaration of competing interest

The authors declare the following financial interests/personal relationships which may be considered as potential competing interests.

Acknowledgments

We thank B. Eggert for the assistance in sample mounting for pressure-dependent VSM measurements. This work has been supported jointly by the Agence nationale de la recherche, project ANR-23-CE09-0031-01 and the Deutsche Forschungsgemeinschaft (DFG), project number 530103526. Partial support by the DFG within CRC/TRR 270, project B02 (Project ID 405553726) and through the Interdisciplinary Center for Analytics on the Nanoscale (ICAN) of the University of Duisburg-Essen, (DFG RIsources reference: RI_00313), the DFG-funded core facility (Project nos. 233512597 and 324659309), are gratefully acknowledged. We thank the European Synchrotron Radiation Facility for provision of synchrotron radiation facilities under the awarded proposal CH 6577 at beamline ID12.

References

[1] Y. Gogotsi (Ed.), MXenes: from Discovery to Applications of Two-Dimensional Metal Carbides and Nitrides, Jenny Stanford Publishing, 2023.
[2] M. Sokol, V. Natu, S. Kota, M.W. Barsoum, On the chemical diversity of the MAX phases, Cell Press 1 (2019) 210–223.

[3] M. Naguib, M. Kurtoglu, V. Presser, J. Lu, J. Niu, M. Heon, L. Hultman, Y. Gogotsi, M.W. Barsoum, Two-dimensional nanocrystals produced by exfoliation of Ti_3AlC_2, Adv. Mater. 23 (2011) 4248–4253.
[4] C. Peng, P. Wei, X. Chen, Y. Zhang, F. Zhu, Y. Cao, H. Wang, H. Yu, F. Peng, A hydrothermal etching route to synthesis of 2D MXene (Ti_3C_2, Nb_2C): enhanced exfoliation and improved adsorption performance, Ceram. Int. 44 (2018) 18886–18893.
[5] W. Sun, S.A. Shah, Y. Chen, Z. Tan, H. Gao, T. Habib, M. Radovic, M.J. Green, Electrochemical etching of Ti_2AlC to Ti_2CT_x (MXene) in low-concentration hydrochloric acid solution, J. Mater. Chem. A 5 (2017) 21663–21668.
[6] V. Kamysbayev, A.S. Filatov, H. Hu, X. Rui, F. Lagunas, D. Wang, R.F. Klie, D. V. Talapin, Covalent surface modifications and superconductivity of two-dimensional metal, Science 369 (2020) 979–983.
[7] M. Li, J. Ku, K. Luo, Y. Li, K. Chang, K. Chen, J. Zhou, J. Rosen, L. Hultman, P.O. A. Persson, S. Du, Z. Chai, Z. Huang, Q. Huang, Element replacement approach by reaction with Lewis acidic molten salts to synthesize nanolaminated MAX phases and MXenes, J. Am. Chem. Soc. 141 (2019) 4730–4737.
[8] K. Arole, J.W. Blivin, A.M. Bruce, S. Athavale, I.J. Echols, H. Cao, Z. Tan, M. Radovic, J.L. Lutkenhaus, M.J. Green, Exfoliation, delamination, and oxidation stability of molten salt etched Nb_2CT_z MXene nanosheets, Chem 58 (2022) 10202–10205.
[9] K. Wang, H. Jin, H. Li, Z. Mao, L. Tang, D. Huang, J.-H. Liao, J. Zhang, Role of surface functional groups to superconductivity in Nb_2C MXene: experiments and density functional theory calculations, Surface. Interfac. 29 (2022) 101711.
[10] X. Xu, C. Zhang, J. Yin, J. Smajic, M. Bahabri, Y. Lei, M.N. Hedhili, M.K. Hota, L. Shi, T. Guo, D. Zheng, J.K. El-Demellawi, M. Lanza, P.M.F.J. Costa, O.M. Bakr, O. F. Mohammed, X. Zhang, H.N. Alshareef, Anisotropic superconducting Nb_2CT_x MXene processed by atomic exchange at the wafer scale, Adv. Mater. (2023) 2305326.
[11] B. Lorenz, C. Chu, High pressure effects on superconductivity, in: A.V. Narlikar (Ed.), Frontiers in Superconducting Materials, Springer, Berlin, Heidelberg, 2005.
[12] L. Zhang, Y. Tang, A.R. Khan, M.M. Hasan, P. Wang, H. Yan, T. Yildirim, J. F. Torres, G.P. Neupane, Y. Zhang, Q. Li, Y. Lu, 2D materials and heterostructures at extreme pressure, Adv. Sci. 7 (2020) 2002697.
[13] X. Dou, K. Ding, D. Jiang, B. Sun, Tuning and indentification of interband transition in monolayer and bilayer molybdenum disulfide using hydrostatic pressure, ACS Nano 7 (2014) 7458–7464.
[14] X.-H. Li, L. Shan-Shan, H.-L. Cui, R.-Z. Zhang, Pressure-induced modulation of electronic and optical properties of surface O-functionalized Ti_2C MXene, ACS Omega 5 (2020) 22248–22254.
[15] H. Jin, K. Wang, Z. Mao, L. Tang, J. Zhang, Structural stability and electronic transport properties of Nb_2C-MXenes under high pressure, Adv. Electron. Mater. 0 (2023) 2201071.
[16] H. Lin, S. Gao, C. Dai, Y. Chen, J. Shi, A two-dimensional biodegradable niobium carbide (MXene) for photothermal tumor eradication in NIR-I and NIR-II biowindows, J. Am. Chem. Soc. 139 (2017) 16235–16257.
[17] H. Dong, P. Xiao, N. Jin, B. Wang, Y. Liu, Z. Lin, Molten salt derived Nb_2CT_x MXene anode for Li-ion batteries, Chemelectrochem 8 (2021) 957.
[18] A. Rogalev, F. Wilhelm, Magnetic circular dichroism in the hard X-ray range, Phys. Met. Metallogr. 116 (2015) 1285.
[19] F. Tran, L. Kalantari, B. Traoré, X. Rocquefelte, P. Blaha, Nonlocal van der Waals functionals for solids: choosing an appropriate one, Phys. Rev. Mater. 3 (2019) 063602.
[20] A. Kokalj, Computer graphics and graphical user interfaces as tools in simulations of matter at the atomic scale, Comput. Mater. Sci. 28 (2003) 155.
[21] A. Eiling, J.S. Schilling, Pressure and temperature dependence of electrical resistivity of Pb and Sn from 1-300K and 0-10 GPa - use as continuous resistive pressure monitor accurate over wide temperature range; superconductivity under pressure in Pb, Sn and, J. Phys. F Met. Phys. 11 (1981) 623.
[22] S. Celerier, S. Hurand, C. Garnero, S. Morisset, M. Benchakar, A. Habrioux, P. Chartier, V. Mauchamp, N. Findling, B. Lanson, E. Ferrage, Hydration of $Ti_3C_2T_x$ MXene: an interstratification process with major implications on physical properties, Chem. Mater. 31 (2019) 454–461.
[23] H. Pazniak, I.A. Plugin, P.M. Sheverdyaeva, L. Rapenne, A.S. Varezhnikov, A. Agresti, S. Pescetelli, P. Moras, K.B. Kostin, A.V. Gorokhovsky, T. Ouisse, V. V. Sysoev, Alcohol vapor sensor based on quasi-2D Nb_2O_5 derived from oxidized Nb_2CT_z MXenes, Sensors 24 (2023) 38.
[24] P.O.Å. Persson, J. Rosen, Current state of the art on tailoring the MXene composition, structure, and surface chemistry, Curr. Opin. Solid State Mater. Sci. 23 (2019) 100774.
[25] S.E. Shadle, B. Hedman, K.O. Hodgson, E.I. Solomon, Ligand K-edge X-ray absorption spectroscopic studies: metal-ligand covalency in a series of transition metal tetrachlorides, J. Am. Chem. Soc. 117 (1995) 2259–2272.
[26] Y. Fan, C. Xu, X. Liu, C. Ma, H.-M. Cheng, W. Ren, X. Li, Distinct superconducting properties and hydrostatic pressure effects in 2D α- and β-Mo_2C crystal sheets, NPG Asia Mater. 12 (2020) 60.
[27] S. Lin, Y. Huang, L. Zu, X. Kan, J. Lin, W. Song, P. Tong, X. Zhu, Y. Sun, Alloying effect on structural, magnetic, and electrical/thermal transport properties in MAX phase $Cr_{2-x}M_xC$ (M = Ti, V, Mn, Fe, and Mo), J. Alloys Compd. 680 (2016) 452–461.
[28] M. Barsoum, MAX Phases: Properties of Machinable Ternary Carbides and Nitrides, Wiley, 2013, p. 436.
[29] R. Khaledialidusti, B. Anasori, A. Barnoush, Temperature-dependent mechanical properties of $Ti_{n+1}C_nO_2$ (n=1,2) MXene monolayer: a first-principles study, Phys. Chem. Chem. Phys. 22 (2020) 3414–3424.
[30] P. Francisco-Santiago, A. Tlahuice-Flores, Ti_2XCl_2 (X = C and N), $TiVCCl_2$ and V_2CFT_x (T_x = F and Cl) MXenes a DFT-D study, Computation and Theoretical Chemistry 1234 (2024) 114525.